Near real-time deforestation detection in Malaysia and Indonesia using Change Vector Analysis with 3 sensors

Pauline Perbet, Michelle Fortin, Anouk Ville, Martin Béland

Department of Geomatics, Laval University, Québec, QC, Canada

Département de géomatique, Université Laval, Québec, QC, Canada

Pauline.perbet.1@ulaval.ca - https://www.researchgate.net/profile/Pauline_Perbet

Michelle Fortin: Research professional - Université Laval

Anouk Ville: Université Laval - UPEM (Université Paris-Est Marne-la-vallée) – ENSG (École nationale des sciences géographiques) Master student

Martin Béland: Ph.D. Research director - Université Laval

Near real-time deforestation detection in Malaysia and Indonesia using Change Vector Analysis with 3 sensors

Malaysia and Indonesia have been affected by deforestation caused in great part by the proliferation of oil palm plantations. To survey this loss of forest, several studies have monitored these southeast Asian nations with satellite remote sensing alert systems. The methods used have shown potential for this approach, but they are limited by imagery with coarse spatial resolution, low revisit times, and cloud cover. The objective of this research is to improve near real-time operational deforestation detection by combining three sensors: Sentinel-1, Sentinel-2 and Landsat-8. We used Change Vector Analysis to detect changes between non-affected forest and images under analysis. The results were validated using 166 plots of undisturbed forest and confirmed deforestation events throughout Sabah Malaysian State, and from 70 points from drone pictures in Sumatra, Indonesia. Sentinel-2 and Landsat-8 yielded sufficient results in terms of accuracy (less than 11% of commission and omission error). Sentinel-1 had lower accuracy (14% of commission error and 28% of omission error), probably resulting from geometric distortions and speckle noise. During the high cloud-cover season optical sensors took about twice the time to detect deforestation compared to Sentinel-1 which was not affected by cloud cover. By combining the three sensors, we detected deforestations about 8 days after forest clearing events. Deforestations were only detectable during approximately the first 100 days, before bare soils were often coved by legume crop. Our results indicate that near real-time deforestation detection can reveal most events, but the number of false detections could be improved using a multiple event detection process.

Keywords: Radar, SAR, optical, Sentinel-1, Sentinel-2, Landsat-8, Forest, Deforestation, Alert, Palm oil, Change Vector Analysis, Multi-temporal, Google Earth Engine, Change Detection

Subject classification codes: Oil Palms

1. Introduction

Interest in palm oil that has been shown by the food industry has grown since the 1950s and has subsequently led to a proliferation of oil palm farms. African oil palm (*Elaeis guineensis* Jacq.) is native to West Africa but has been naturalised in the rest of the continent, the Caribbean basin, Brazil, and Southeast Asia. The high yield and low cost of the edible vegetable oil that is extracted from this palm species has encouraged its widespread cultivation. The sharp increase in the extent of these plantations has resulted in deforestation across large tracts of land in Malaysia and Indonesia (Hansen et al. 2008; Rival and Levang 2013; Awalludin et al. 2015). Limiting deforestation is a global issue that is related to the carbon cycle (Koh et al. 2011; Khun and Sasaki 2014), climate change (Houghton et al. 2015), biodiversity, and habitat conservation (Rival and Levang 2013). High demand for this cheap cooking product also continues to incur certain social costs (Wakker et al. 2004). Consumers, and by extension, the palm oil producers and buyers up the production chain, are more engaged today in implementing deforestation-free oil production (May-Tobin et al. 2012). There is an urgent need to devise strategies that would sustain a responsible oil palm industry. For this reason, a dynamic system that targets deforestation could potentially be a valuable tool for managers who wish to improve the traceability of palm oil.

One of the most efficient ways of achieving near real-time observations across a large study area is through remote-sensing satellite-based monitoring (Hansen and Loveland 2012; Reiche et al. 2018). Operational deforestation-alert systems that are based on remote sensing have been implemented in several studies over the last few years. Most results are freely available from Global Forest Watch (http://www.globalforestwatch.org). Typically, Landsat-8 imagery is employed, with 30 m resolution and new coverage of a given region every 16 days (Hansen et al. 2016). The imagery provided by the

MODIS (Moderate Resolution Imaging Spectroradiometer) sensor has a resolution of 250 m, with near-daily re-visitation (Reymondin et al. 2012; Hammer et al. 2014; Wheeler et al. 2018). Because of its coarse resolution, MODIS tends to miss smaller deforestation events, whilst Landsat-8 is limited by its low temporal frequency of re-visitation (Hansen and Loveland 2012). Another existing monitoring system is the Starling service from Airbus Defence and Space, and its partners (http://www.starling-verification.com), which uses SPOT (Satellite Pour l'Observation de la Terre) 1.5 m resolution images to create land cover maps and allow palm oil companies to self-verify that they are honouring their commitments to limiting deforestation.

The main constraint facing all optical observations in tropical areas is persistent cloud cover, especially in high elevation areas that experience few cloud-free days throughout the year, therefore limiting remote sensing opportunities (Hansen et al. 2016). Adding radar images to the monitoring process may improve the detection of deforestation under cloud cover (Berry et al. 2010; Joshi et al. 2016; Reiche et al. 2018). Yet, radar processing is challenging due to geometric distortion (foreshortening, layover and shadowing) and speckle noise (Lê 2015; Joshi et al. 2016). Moisture variation and the surface roughness of bare soil can also lead to large changes in backscatter responses (Berry et al. 2010). Some studies have recently confirmed the interest of combining optical and radar sensors to improve the accuracy of detecting deforestation (Reiche et al. 2018, Lehmann et al. 2015).

Deforestation events are observable in optical images by sudden changes in reflectance. In radar images, the difference in roughness between the forest and the bare soil affects the backscatter response. The spectral response of deforestation varies in relation to the type of land-clearing techniques that are employed. The largest industrial farms use

machines for grubbing and swathing to clean large areas (Surre and Ziller 1963). Small farmers prefer to use traditional slash-and-burn techniques because of their low costs (Jacquemard 2013). The soil following deforestation can also exhibit different responses, relative to the progress in plantation preparation at the time of imaging. Site preparation includes the creation of a circulation lane and a drainage system (Verheye 2010). In most plantations, legume cover crops are planted to prevent soil erosion, and to quickly cover the bare soil by vegetation. Forest-clearing operations are mainly conducted during the driest season, to make room for planting at the beginning of the rainy season (Verheye 2010). Once bare soil is covered and no longer visible to optical sensors, deforestation may not be detected. Palm oil plantations are usually cleared and replanted at the end of the 25-year productive cycle of palm trees (Verheye 2010).

The objective of this work is to improve the resolution, and the temporality of real-time deforestation monitoring by combining Landsat-8, Sentinel-2 optical sensors, and Sentinel-1 radar sensor. The detection response of each sensor is analysed to determine benefits between active (radar) and passive (optical) sensors. Results are analysed in regard to the field surface conditions during the clearing and planting processes in order to understand the source of detection errors. As this work aims to contribute to an operational monitoring system to aid in oil traceability, we also aim to describe the temporality of alerts in terms of the responsiveness of the first alert, and the frequency of detection. Moreover, the operational system being developed demands greater consistency in terms of user accuracy, and therefore we analysed the causes of false detection events.

2. Materials and methods

2.1. Study Area

The study focuses on two areas shown in Figure 1(a). The first area covers the State of Sabah, Malaysia. Sabah occupies the northern portion of the island of Borneo and covers about 74,000 km². The second, is a 442 km² area located on the island of Sumatra, Indonesia between Bukit Tigapuluh National Park and the city of Jambi.

Sabah's natural forests are mostly composed of mixed Dipterocarpaceae, peatlands, and mangroves (Bryan et al. 2013). In 2017, about 15500 km² had been replaced by oil palm plantations, corresponding to over 20 % of the state's area (Malaysian Palm Oil Board 2017). In 2017, only 59 % of the natural forest in Sabah remained (Asner et al. 2018). Bryan at al. (2013) calculated that more than half of the remaining forest had been degraded or severely degraded by selective logging and roads. Using different methods, Gaveau et al. (2016) made an estimate of forest impacts that was of a similar order of magnitude to the previous estimate (Bryan et al. 2013). These logged and degraded forests are still considered important for protecting biodiversity, because of their high carbon stocks (Asner et al. 2018) and other interests that are associated with these habitats (Evans et al. 2018).

Sumatra had about 59000 km^2 cover of oil palm plantation in 2015 (Austin et al. 2017). Peatland are particularly impacted, with 33.3% converted to industrial plantation in 2015 (Miettinen et al. 2016).

As is the case with all tropical regions, our study areas are affected by persistent cloud cover. During a high cloud-cover season, (December to March) 50 % of pixels on Sabah can be covered by clouds, compared to a low cloud-cover season (April to November) (Figure 1(b)).

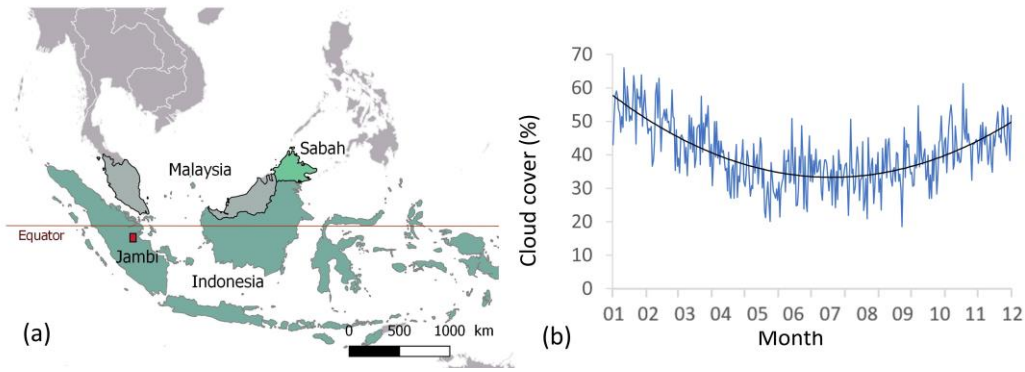

Figure 1: (a) Study area locations, (b) Daily percentage cloud cover and the polynomial trend line for Sabah, which was calculated from 10 years of MODIS surface reflectance products 'state_1km', MODIS, MOD09GA, 2017 (Vermote and Wolfe 2015).

2.2. Data

2.2.1. Sensors and Google Earth Engine

Landsat-8 is a sensor platform that is commonly used in change detection, while Sentinel-1 and Sentinel-2 are relatively new satellites (launched by the European Space Agency in 2014 and 2016, respectively). Their respective periods of availability over the Malay Archipelago are shown in Figure 2. Revisit times are 16 days for Landsat-8, 10 days for Sentinel-1, and 5 days for Sentinel-2 (combining S2A and S2B), respectively. An operational near real-time alert system requires a frequent revisit. It is advantageous to analyse all available images of these three sensors, resulting in a high volume of data collection. By using the Google Earth Engine (GEE) system, the data in a cloud catalogue that is continuously updated can be readily accessed. GEE combines a remote sensing imagery catalogue with a computational infrastructure and algorithms capable of conducting various types of analyses. Optical images are pre-processed for top of atmosphere (TOA) reflectance calibration and co-registration. For Sentinel-1, GEE uses the ESA (European Space Agency) Toolbox to generate a calibrated, ortho-corrected Sentinel-1 collection. GEE is a web platform optimized to perform per-pixel

operations (Gorelick, 2017). Sentinel-2 and Landsat-8 are globally misaligned by approximately 38 m (Storey et al. 2016). We analyzed more than 30 points throughout our study area which were previously projected at 30 m, and the impact of the misalignment was considered negligible on Sabah and Sumatra.

We used data from 1 January 2017 to 31 May 2018 for the overall Sabah region to provide enough validation samples in both high cloud-cover and low cloud-cover seasons. A total of 1824 images were collected throughout the 17 months period (210 Landsat-8, 1328 Sentinel-2 and 286 Sentinel-1).

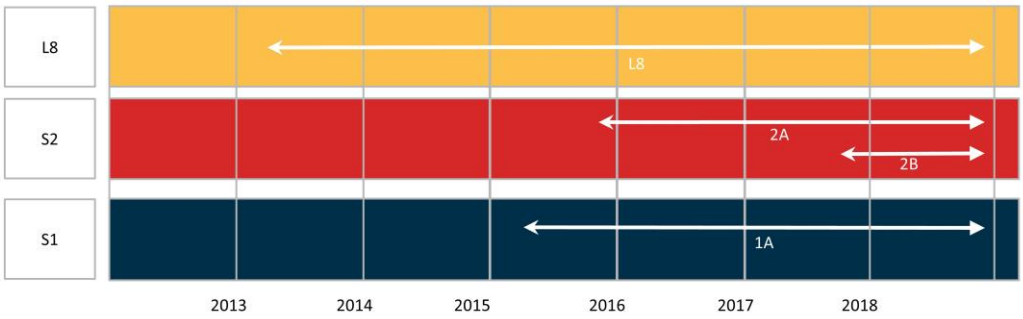

Figure 2: Availability of images over Malaysia and Indonesia for Landsat-8, Sentinel-1 and Sentinel-2.

2.2.2. Training and validation samples

To identify the status of the surface conditions within training and validation plot samples, we used recent high-resolution images that were made available online by the planet.com platform (Planet 2018). This commercial satellite operator uses over 175 PlanetScope satellites (CubeSat type) to capture daily images of 3 metres resolution, which have been orthorectified all around the globe (Houborg et al. 2018).

To determine thresholds of the detection method, we searched for and identified 15 deforestation events throughout the Sabah area. These deforestation events were found

by searching through the planet.com imagery, and the evolution of the surface conditions evolution through time was fully documented.

For validation purposes, we used stratified random sampling throughout the Sabah state. The 71 deforestation polygons (average size of 0.7 ±1.1 ha) were defined throughout 2017 and early 2018, by photo-interpretation research in planet.com imagery. We assured the initial land cover type was forest using high resolution Google Earth images. Then, 98 polygons visually identified as intact forests in May 2018 (average size of 27 ±22 ha) were randomly selected in planet.com imagery (including dipterocarp forests, peatlands and mangroves).

The planet archive web platform associated with Sentinel-2 and Landsat-8 time series allowed us to estimate the deforestation date for each training and validation polygon. These dates have a slight bias, because of the delay between deforestation and the available cloud cover-free imagery. This bias is difficult to estimate, partly because PlanetScope satellites revisits are irregular.

2.2.3. Drone samples

Drone photographs were obtained from a field survey (8 and 9 May 2018) that was conducted in Sumatra between Bukit Tigapuluh National Park and the City of Jambi. From the photographs, we determined validation points and classified them as intact forest (27 points) or forest cover losses (43 points), for a total of 70 points. This second site was useful for observing the state of the soil surface and understanding the omission of deforestation events.

2.3. Methods

The methodological approach we used can be summarised as follows: (1) image pre-

processing, (2) establishment of the forest reference, (3) Change Vector Analysis (CVA) application to all new images, and (4) application of appropriate thresholds to detect deforestation events (Figure 3).

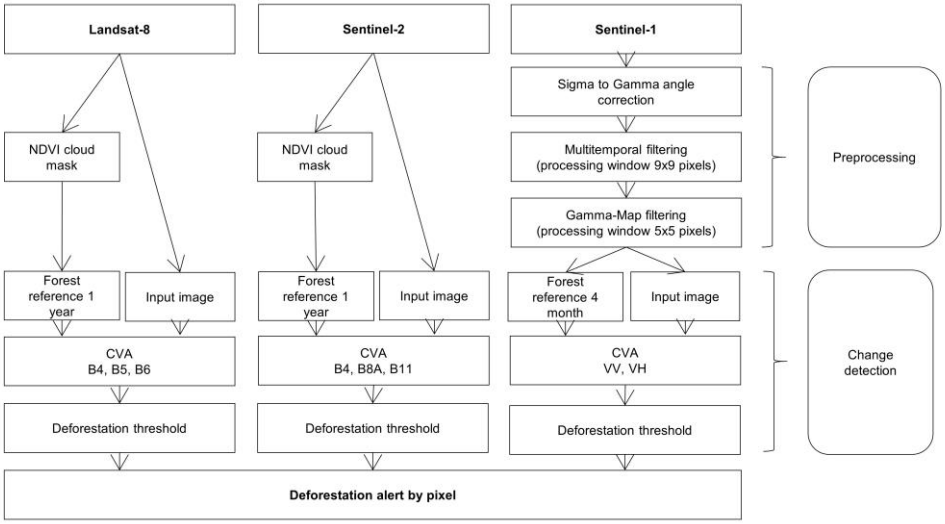

Figure 3: Analysis method flowchart. The method performs the simultaneous analyses of three sensors to detect deforestation.

2.3.1. Image preprocessing

2.3.1.1. Optical Sensors

Sentinel-2 and Landsat-8 optical images were already converted to TOA reflectance by GEE. No atmospheric correction was applied to the images. According to Song et al. (2001), training data from large areas and from different times of the year allow for avoiding atmospheric correction processes. Because the study area is located in humid tropical forest, we observed that phenological events are much more subtle than the noticeable seasonal changes in forest cover that regularly take place in drought-deciduous tropical forest or in temperate deciduous forest. Therefore, no seasonal filters were employed in the current study.

2.3.1.2. Radar Sensor

For Sentinel-1 images, images should be filtered to decrease speckle noise (Lê 2015), especially because CVA is a pixel-based comparison. Filters should conserve temporal and geometric information of deforestations. We decided to use a double filter approach as suggested by Quegan et al (2000). While with times series, a multi-temporal filter gives the advantage of preserving edges. The one-stage multi-temporal filter did not provide enough classification performance accuracy compared to that of two-stage multi-temporal and spatial filters (Quegan et al. 2000, Maghsoudi et al. 2014). Three steps were required for this pre-processing: (1) Gamma transformation; (2) Multi-temporal despeckle filter; and (3) and Gamma-map filter. (1) The gamma transformation that is expressed by the following formula is a process that considers the angle of incidence that varies from one side of an image to the other:

$$\gamma^0 = \frac{\sigma^0}{\cos\theta} \quad (1)$$

where gamma (γ) is the transformed pixel value in dB, sigma (σ^0) is the initial pixel value in dB, and theta (θ) is the incidence angle, in radians.

(2) The multi-temporal despeckle filter (Quegan et al. 2000), acts in over a spatial and temporal domain. This filter reduces speckle by relying upon information that is common to different dates, and while preserving the temporal information contained in each image. The multi-temporal filter code has been implemented with the help of the GEE help forum community. (3) The Gamma-map filter (Lopes et al. 1990), is an adaptive spatial filter, which smooths the homogeneous zones while preserving edges.

2.3.2. The forest references

References represent the time average signals of non-affected forest pixels, which are

compared with each new image in order to determine whether a change has occurred or not. To create forest references, we filtered out clouds from the Sentinel-2 and Landsat-8 images. We found that cloud masks that were available in GEE missed several clouds and shadows, therefore, we designed a simple mask from conventional normalised vegetation index (NDVI; Rouse et al. 1974). NDVI values below 0.6 were found to mostly refer to clouds and shadows, but they also included bare soil, urban areas, and water; vegetation pixels were mostly excluded. To obtain complete cover for the forest reference throughout the study area, we averaged all images for the previous year (2016). In contrast, Sentinel-1 images are not affected by cloud cover, therefore, we averaged only one month (December 2016) of pre-processed images to obtain the reference.

2.3.3. Change vector analysis

Our research applied Change Vector Analysis over the 3 sensors to detect the deforestation. CVA is a change detection per pixel method that is commonly used with optical images (Phua et al. 2008; Fernandes et al. 2014), but it is an innovative approach in the use of radar. Indeed, speckle noise of the radar sensor makes it difficult to implement the change detection process per pixel (Qi et al. 2015). To overcome the issue, the speckle noise was properly minimized by the pre-processing filters.

For each pixel, we calculated the magnitude and the direction of change between the forest reference image and a new image (Malila 1980; Thonfeld 2016). The magnitude is the Euclidean distance between the spectral values of 2 images that are positioned in 3-band spectral space. This length indicates the presence of change between the initial image and the new image. The direction is the angle projected in all the axes (Figure 4). The direction of change provided the change type, i.e. whether it is a cloud, a shadow or

a deforestation event. To allow visual interpretation, we separated each pair of bands for the angle calculation. Formulae that were used for these calculations are:

$$\mu = \sqrt{(\Delta R_{\mathrm{Y}})^{2} + (\Delta R_{\mathrm{X}})^{2} + (\Delta R_{\mathrm{Z}})^{2}} \quad (2)$$

$$\alpha = \mathrm{arctg}\left(\frac{\Delta R_{\mathrm{Y}}}{\Delta R_{\mathrm{X}}}\right) \text{ and } \mathrm{arctg}\left(\frac{\Delta R_{\mathrm{Z}}}{\Delta R_{\mathrm{X}}}\right) \text{ and } \mathrm{arctg}\left(\frac{\Delta R_{\mathrm{Z}}}{\Delta R_{Y}}\right) \quad (3)$$

where (2) μ is the magnitude of change, and (3) α is the direction of change. ΔR_{Y} is the difference between the spectral value of 2 images for band Y, ΔR_{X} is the difference between the spectral value of 2 images for band X. If a third band is used, ΔR_{Z} is the difference between the spectral value of 2 images for band Z. Radiometric bands or polarization bands X, Y and Z were defined, depending upon the sensor.

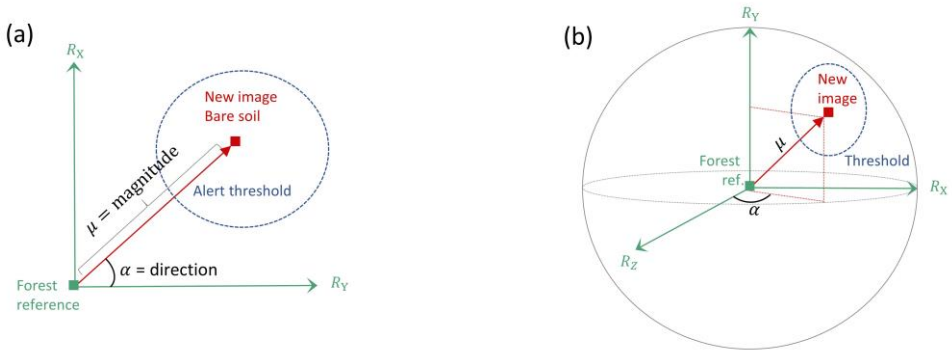

Figure 4: (a) Representation of change vector in two-band radiometric change space (for Sentinel-1), (b) Representation of change vector in three-band radiometric change space (for Sentinel-2 and Landsat-8).

A great advantage of using CVA is that clouds and shadows are detected as a specific change, consequently we did not have to processing cloud masks for each new input image.

To facilitate visualisation and interpretation, we used 3 bands to process the vector analyses for the optical images. Change information could also be located in other bands, but after analysed correlation between the bands, we found that 3 bands were sufficient. The red, near-infrared (NIR) and Shortwave Infrared (SWIR) bands were chosen for deforestation detection because of their ability to strongly segregate forests

or clouds from bare soil. We used similar bands between Landsat-8 and Sentinel-2. For NIR, B8A from Sentinel-2 was used, because it is closest to band 5 of Landsat-8 (Mandanici et al. 2016). Red was defined by band 4 for the two sensors, while SWIR was defined by band 6 in Landsat-8 and by band 11 for Sentinel-2, respectively.
To find the threshold on magnitude and angles for the optical sensor, we created seven classes of change: no change (forest stays forest), deforestation (forest became bare soil), various fog-covered forest, various fog-covered bare soil, regrowth (new vegetation in bare soil), various clouds, and various shadows. For the Sentinel-1 radar sensor, we focused on 2 classes of change; no change (forest stays forest) and deforestation (forest became bare soil), determined from the image date against date of deforestation.

The length and three angles between the forest reference and deforestation were calculated and displayed in a polar coordinate plot as a function of change class to determine the best alert threshold for each angle combination (Figure 5). For the Sentinel-1 radar sensor, we used polarization bands available, VV and VH, to find the length and angle of the vector.

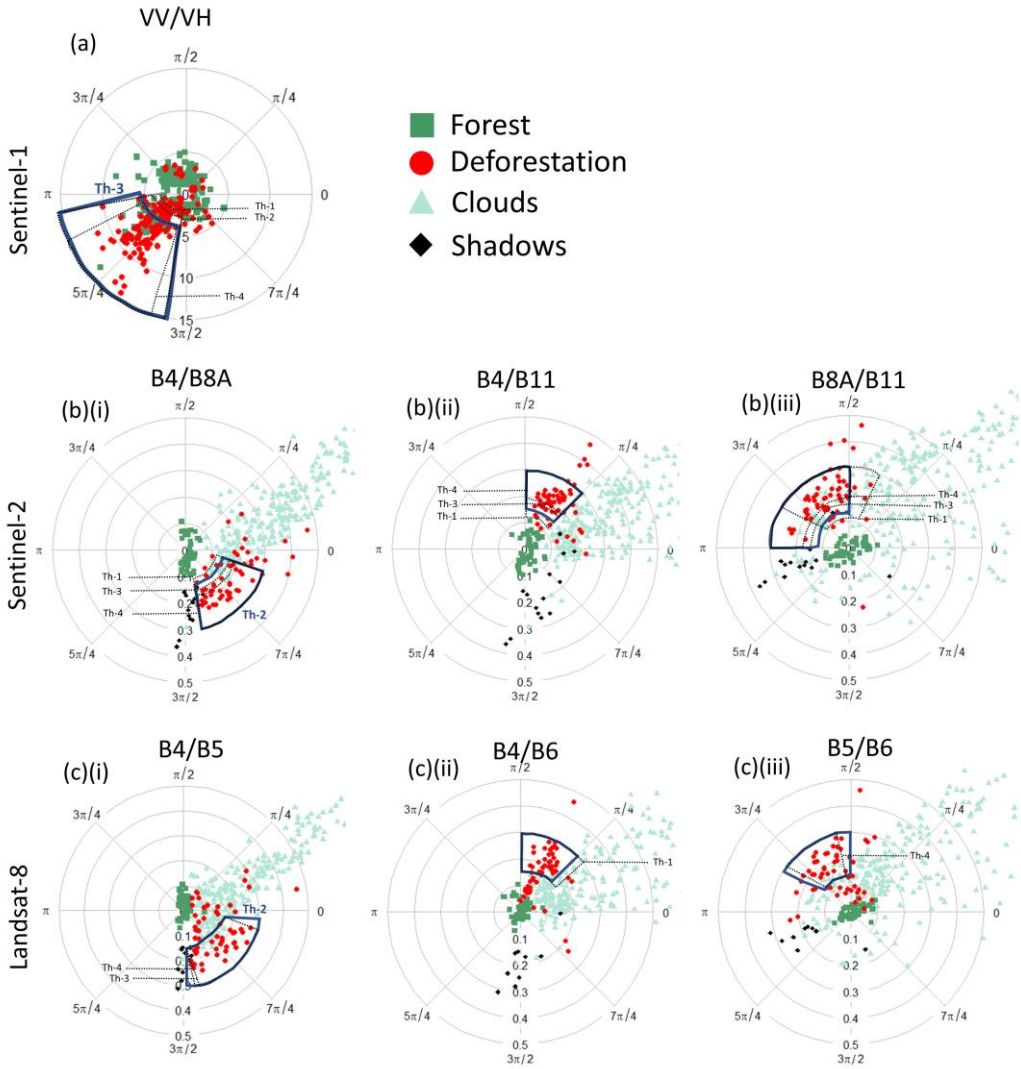

Figure 5: Figure (a) illustrates the VV (vertical/vertical) and VH (vertical/horizontal) bands for Sentinel-1. Figure (b) corresponds to Sentinel-2 sensors, with (b)(i) angle Band 4/Band 8A, (b)(ii) angle Band 4/Band 11 and (b)(iii) angle Band 8A/Band 11. Figure (c) corresponds to Landsat-8 sensors, with (c)(i) angle Band 4/Band 5, (c)(ii) angle Band 4/Band 6 and (c)(iii) angle Band 5/Band 6. Polar coordinate plots that were obtained by applying CVA, against 15 reference forest polygon averages. Green represents no change, red represent deforestation events, and blue are samples covered by cloud. The blue polygon indicates the deforestation threshold. Black dash polygons represent other examples of thresholds.

2.3.4. Threshold to detect deforestation

To identify the optimal detection rate, we used a trial-and-error approach. We selected the threshold where most of the polygons were detected and contained a low false detection rate (figure 6), which is essential for real time alert purposes (Reiche and all.

2018). Bands used for Sentinel-2 are the same as for Landsat 8 (Mandanici et al. 2016), but we found different thresholds for the two sensors.

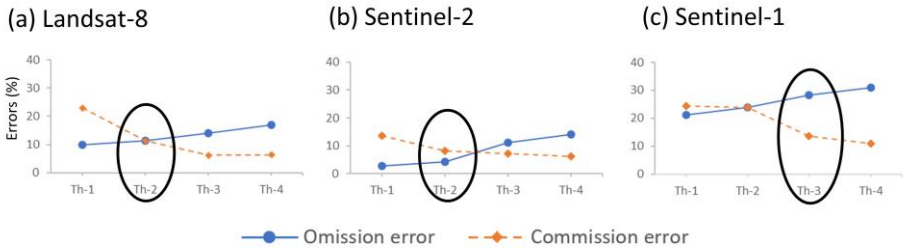

Figure 6: Spatial accuracy (omission and commission errors) of the deforestation class as a function of four examples of threshold values, separately for (a) Landsat-8, (b) Sentinel-2 and (c) Sentinel-1. Thresholds annotation correspond to the parameters shown in Figure 5. Surrounded thresholds were used in our study.

Once the decision tree triggered the alert, the individual results are merged together to obtain a single image with all pixels detected as deforestation during the study period. This combination is performed for each sensor and at multi-sensor level.

The change detection algorithm was coded in Google Earth Engine and applied throughout the Sabah state between 1 January 2017 and 31 May 2018 (Figure 7).

Two approaches were used to evaluate results: (1) A polygon level approach is analysed by deforestation events. When at least one pixel was found inside the validation polygon we considered the deforestation event to be detected. If one pixel was tagged as deforestation inside an undisturbed forest polygon, the polygon was tagged as a false detection, and (2) A pixel-based approach to measure the capacity of detecting at small scale deforestation. The pixel accuracy is adjusted according to the proportion of each class in Sabah (Olofsson 2014).

Only the pixel-based approach method was applied over the Sumatra area of interest between 1 January 2018 and 31 May 2018 (Figure 7).

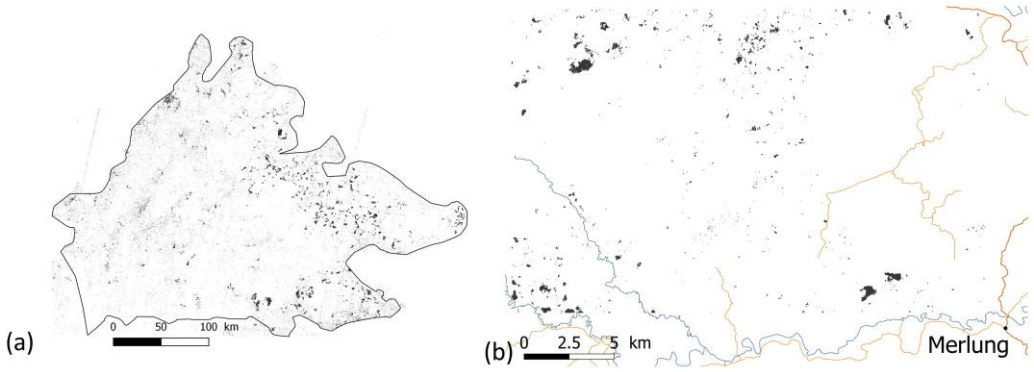

Figure 7: (a) Deforestation events detected at the multi-sensor level during the 17 months monitoring period in Sabah. (b) Deforestation events detected at the multi-sensor level during the 5 months monitoring period in Sumatra study area.

3. Results and discussions

3.1. Change detection accuracy

With regards to the polygons level approach, the three sensors had a high consensus of accuracy (Figure 8). Sentinel-1 showed the highest degree of omission error (20 polygons undetected) compared to optical sensors, which detected more deforestation events. Sentinel-2 and Landsat-8 showed best results with commission errors of 4 % and 11 % respectively. In the pixel focus, all sensors had a higher omission error, which showed that only a relatively small number of pixels had been detected for each deforestation event. However, after combining the 3 sensors, the omission error decreased to 6%.

Sentinel-1 had greater commission error than the optical sensors. Sentinel-2 and Landsat-8 performed better in relation to the commission error in the pixel approach compared to the polygons focus, which showed that only a few pixels were false detected.

A final result combining all the sensors from the 17 months study period was compared with the GLAD (Global Land Analysis & Discovery) alert system during that same time frame (Hansen et al. 2016) (Figure 8). With 6% of omission error, our method provides a better detection of the deforestation pixel than GLAD (37% of omission error). On the other hand, the GLAD alert generates fewer false detections (3% of commission error).

False detections that occurred in intact forest were mainly due to artefactual pixels located at the border of the tiles for Sentinel-1 or Sentinel-2. Further, half of the forest polygons corresponding to mangrove (10% of our plots) were detected as false detections. Excluding mangrove from the study area would have likely improved the commission error. We observed that false detections typically occurred up to 3 times per polygon during the entire study period.

Of the 71 deforestation validation polygons, only 3 were omitted by Sentinel-2. Landsat-8 missed 8 polygons during the analysis period. Only two deforestations event were not detected by any sensor. The spectral response of those events could be different, due to soil type or the progress of field preparation.

Sentinel-1 yielded the poorest statistical results, likely a consequence of its geometric distortion and speckle noise not completely corrected by preprocessing filters. In addition, moisture and roughness variation of the bare soil during the plantation process can create difficulties to detect deforestation events. Comparatively to optical sensors, radar was not as valuable for detection deforestation.

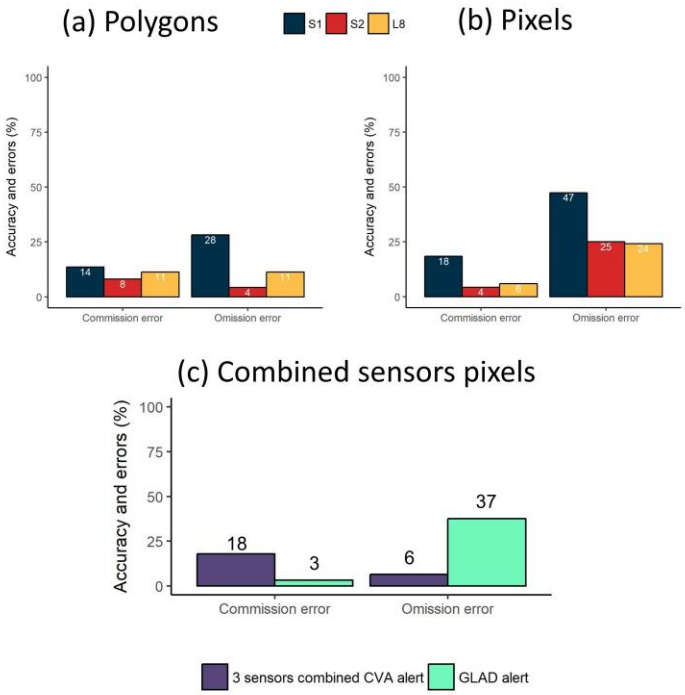

Figure 8: Comparative analysis of deforestation omission, and commission error for the three sensors corresponding to the best thresholds. (a) Corresponds to the polygons level approach, and (b) to the pixel-based adjusted area. (c) Represent the multi-sensor analysis in pixel-based adjusted area and its comparison with GLAD alert detection (Hansen et al. 2016). Numerical values on the histogram bars represent exact percentage values.

3.2. Detection responsiveness as a function of cloud cover

Sabah is characterised by a high cloud-cover season between December and March, which affects optical images (Figure 1). We compared the reaction time for detecting deforestation as a function of the density of cloud cover (Figure 9). Based upon known deforestation dates, 9 polygons were deforested during the high cloud-cover season, while 54 were defined as low cloud-cover season. Results show that Sentinel-1 detection delay was of a similar order of magnitude throughout the year. Optical sensors more than doubled the time period for the first detection during the peak cloudy season. During low cloud-cover season, Landsat-8 attained first detection at around 11.5 days. The median of first detection is 8±4.6 days, when we combined all sensors throughout the study period.

These results support the relevance of including Sentinel-1 in near real-time detection of deforestation events throughout the year in areas subject to high cloud cover.

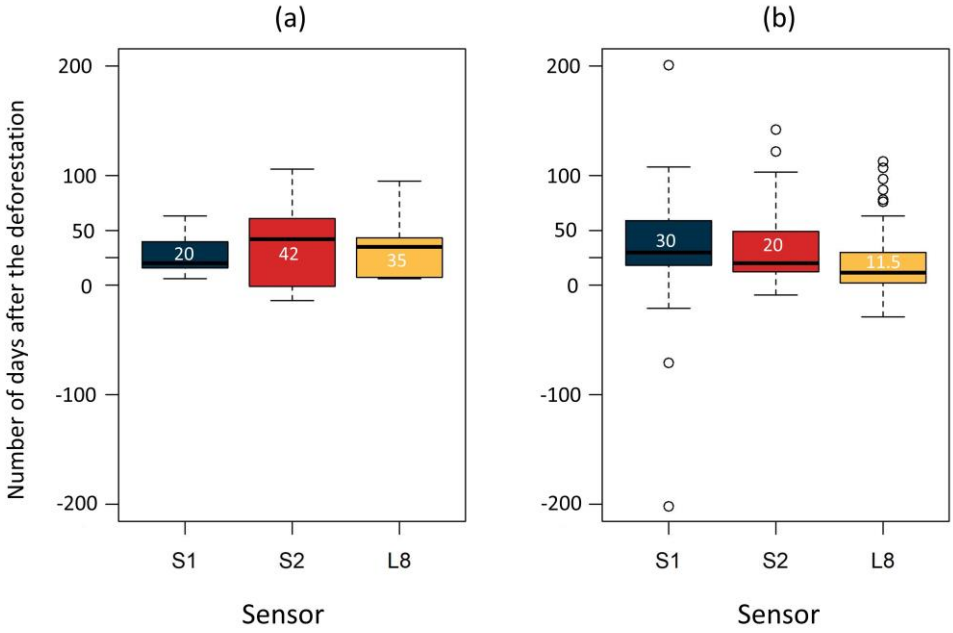

Figure 9: Days of the first detection after deforestation events (estimates) across sensors, for (a) high cloud-cover season and (b) low cloud-cover season. The thick horizontal line within the box-plots represents the median (50th percentile) of each sensor. The box-plots themselves delimit the first and third quartiles (25th and 75th percentiles) and the whiskers (vertical dashed lines) indicate the 10th and 90th percentiles. Open circles represent outliers (i.e. values that are beyond 1.5 times the interquartile range.

3.3. Temporal evolution of detection

Most deforestation events were detected between 0 and 100 days after the disturbance (Figure 10). After 100 days (over 3 months), the number of detections decreased until 300 days (10 months) had passed, after which polygon deforestation events were no longer detected.

Dynamic cover crop species can completely cover soil 4 to 5 months after the plantation (Skerman 1982), and this dynamic growth rate is consistent with the decrease of the detection of bare soil after 3 months.

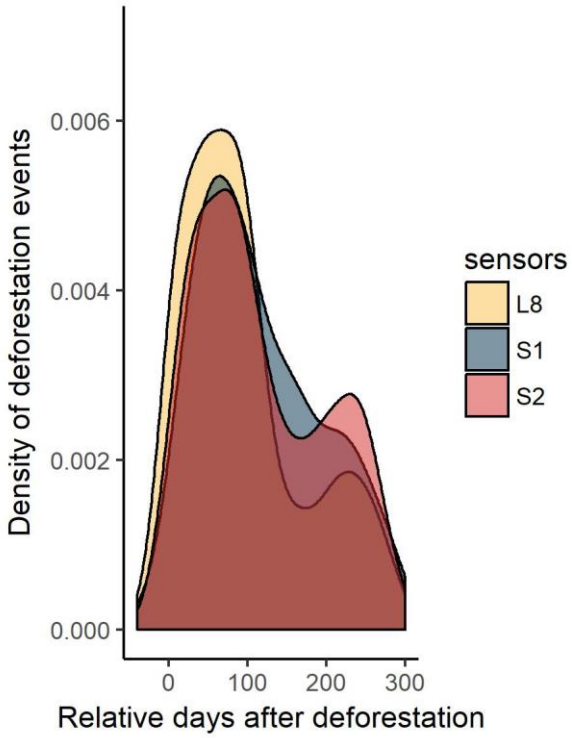

Figure 10: Density of deforestation events that were detected as a function of time following deforestation (estimated). These results allowed us to visualise the distribution of detection responses before and after deforestation. Zero is the estimated first date of forest cover loss.

3.4. Frequency of detection

For an operational detection system, false detection must be avoided as much as possible. False detections were found to be mostly due to artefact in the imagery and occurred a maximum of 3 times per validation polygon in a period of 17 months. Hence, to confirm a deforestation event, pixels should be detected at least 3 times to eliminate the potential for random errors. We wondered if deforestation events were detected frequently enough to allow this confirmation. The number of validation polygons (as percentages) are presented in Figure 11 as a function of the number of times that they were detected over a period of 100 days following forest clearing. Two of the 71 polygons were never detected during the analysis interval, and three others were only detected once; 18 % of the validation polygons were detected fewer than 4 times, while half of the polygons were detected less than 11 times each. This frequency was possible

because detection results from all three sensors were used, thereby supporting the interest of combining radar and optical sensors in this context.

The accumulation of 3 detections to reduce commission error increases the omission error rate to 24% and decreases the commission rate to 1% (instead of 6% of omission error and 18% of commission error).

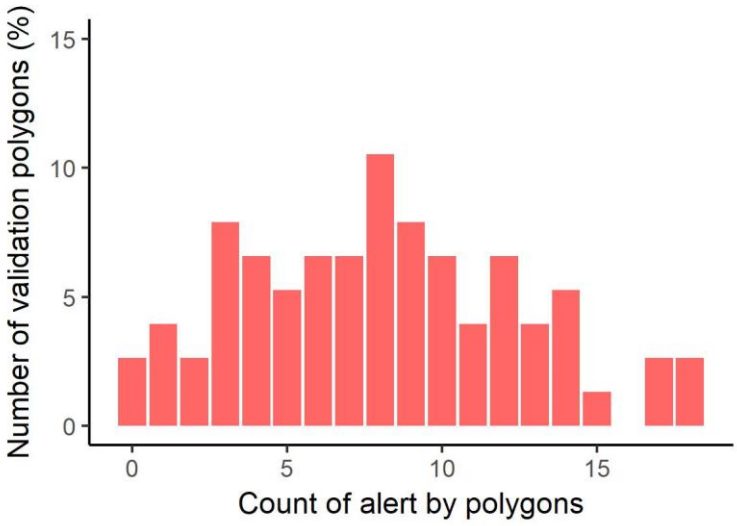

Figure 11: Number of validation polygons (as percentages) as a function of the number of times that they were detected over a period of 100 days following forest clearing.

3.5. Validation in Sumatra

We implemented our detection method in the Sumatra area between 1 January and 31 May 2018 (Figure 12). We estimated that this period should correspond to the deforestation events of areas captured by drone imagery in early May. Results from confusion matrix (Figure 13) yielded a high number of omission errors (53 %) in deforestation detection. None of the 29 forest points were detected as false detections (commission error of 0%). The low number of results could be attributed to a delay between deforestation events and alert detection being too short if the deforestations occurred in early May, or by the state of the forest before the disturbance. Indeed, about 10 points had not been detected by our method but appeared to be bare soil in the

imagery. However, these areas have been previously disturbed and did not represent undisturbed forest canopy. This result show that our methodology is well oriented to only detect disturbance of intact forests.

We compared our results against the GLAD alert system (Hansen et al. 2016). We applied the confusion matrix to our field plots versus possible GLAD alert pixels. Most points were not detected by the GLAD system (omission error of 86 %) compared to our method. Both methods demonstrated no commission error.

When we confined the use of our method to Landsat-8 only, we obtained results that were similar to the GLAD alerts (omission error of 81 %). This comparison suggests there is high relevance in using the three sensors for improving the change detection process in these forested areas.

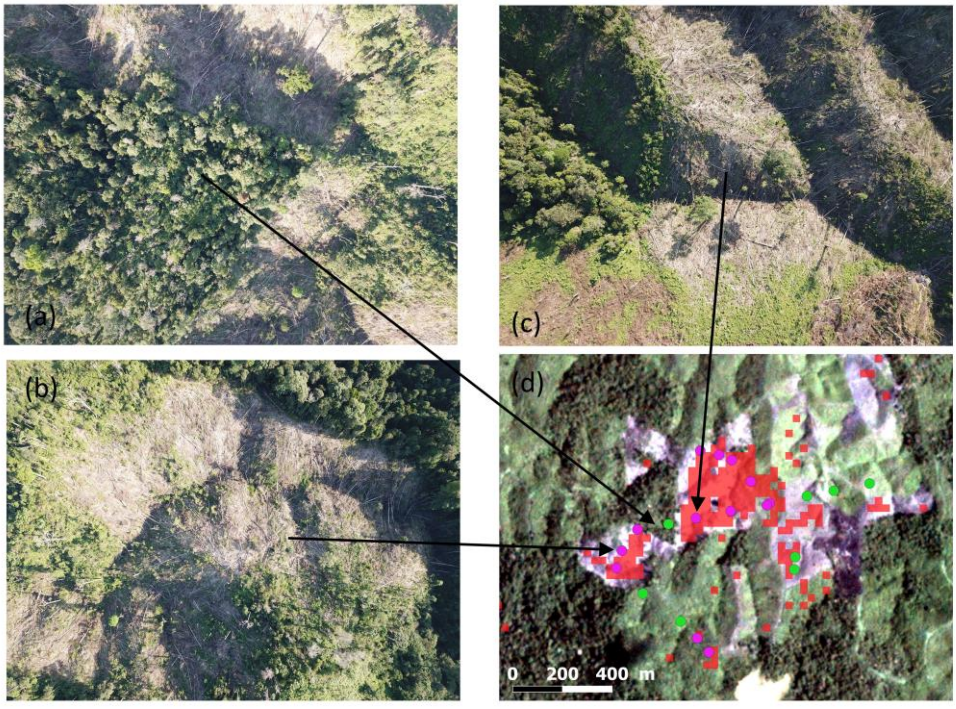

Figure 12: (a, b, c) Examples of drone photographs that were taken 9 May 2018. (d) Illustration of deforestation detection: In red, pixels detected as deforested by our method, between 1 January and 31 May 2018, over a Planet image of 18 February 2018. Points are the position of the drone pictures, green points are forest (a), and pink points are bare soil (b and c).

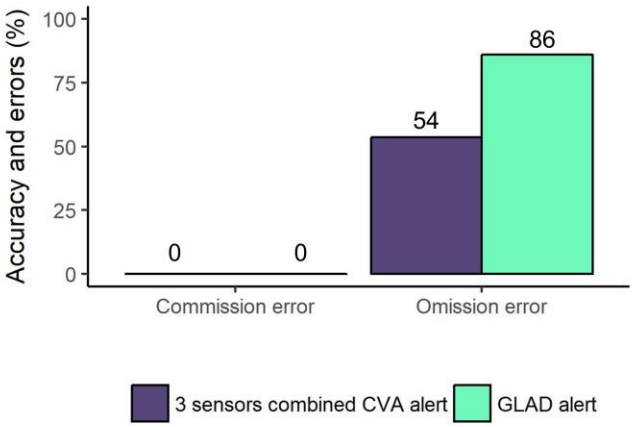

Figure 13: Figure 13. Comparative analysis of deforestation omission and commission errors and overall accuracy of the method presented in this paper versus that provided by GLAD forest alert detection (Hansen et al. 2016). Numerical values on the histogram bars represent exact percentage values.

4. Conclusion

The objective of this research was to assess to what extent could we improve near real-time deforestation observations by combining Landsat-8 and Sentinel-2 optical sensors, and the Sentinel-1 radar sensor over Southeast Asia. By using Change Vector Analysis method over Sabah, Malaysia, all sensors separately yielded reasonable statistical results. With 14% of commission error and 28% of omission error, we consider the Change Vector Analysis method in detecting deforestation effective with Sentinel-1, despite speckle noise. A comparison between our method (yielding 54% omission error) and the GLAD alert system (86% omission error) (Hansen et al. 2016) in a smaller area in Sumatra, confirms the utility of combining the three sensors for improved detection. Sensors have different characteristics, which can provide a high-performance operational system when used together. By comparing pixel and polygon metrics errors, we observed that only a small part of the deforestation was detected by each sensor, and the combination allowed for better detection (6% of omission error). Sentinel-2 and Landsat-8 data are more accurate in the detection of deforestation events. During high cloud-cover season, while optical sensors took about twice the time to detect

deforestation, the reaction time of Sentinel-1 remained about 20 days. Using of the three sensors provided informative detection results during the first 100 days after the deforestation event, before bare soils were covered by legume crop. Almost every deforestation event was detected by our method (97%), but results were affected by several false detections (25%) mostly generated by imagery artefacts. Those false detections could be avoided by adding a system of confirmation using multiple detections per pixel.

Acknowledgements

We gratefully acknowledge the anonymous reviewer for the relevant comments provided. The Natural Sciences and Engineering Research Council of Canada (NSERC) provided support this project (grant 484231-15). Thanks to William F.J. Parsons for the English editing of this paper, funded by the Centre for Forest Research. Gratitude to Andre Beaudoin, Canadian Forest Service, for his advices on the radar filtering process.

References:

Awalludin, Mohd Fahmi, Othman Sulaiman, Rokiah Hashim, and Wan Noor Aidawati Wan Nadhari. 2015. “An Overview of the Oil Palm Industry in Malaysia and Its Waste Utilization through Thermochemical Conversion, Specifically via Liquefaction.” *Renewable and Sustainable Energy Reviews* 50 (October): 1469–84. https://doi.org/10.1016/j.rser.2015.05.085.

Asner, Gregory P., Philip G. Brodrick, Christopher Philipson, Nicolas R. Vaughn, Roberta E. Martin, David E. Knapp, Joseph Heckler. 2018. “Mapped aboveground carbon stocks to advance forest conservation and recovery in Malaysian Borneo”.

Biological Conservation, 217 (January) 289-310
https://doi.org/10.1016/j.biocon.2017.10.020

Austin, K. G., A. Mosnier, J. Pirker, I. McCallum, S. Fritz, and P. S. Kasibhatla. 2017. "Shifting Patterns of Oil Palm Driven Deforestation in Indonesia and Implications for Zero-Deforestation Commitments." Land Use Policy 69 (December): 41–48. https://doi.org/10.1016/j.landusepol.2017.08.036.

Malaysian Palm Oil Board, Economics and Industry Development Division: http://bepi.mpob.gov.my/index.php/en/statistics/area.html - Accessed june 2018

Berry NJ, Phillips OL, Lewis SL, Hill JK, Edwards DP, et al. 2010. "The high value of logged tropical forests: lessons from northern Borneo." *Biodiversity Conservation* 19: 985–997.

Bryan, J.E., Shearman, P.L., Asner, G.P., Knapp, D.E., Aoro, G., et al. 2013. "Extreme Differences in Forest Degradation in Borneo: Comparing Practices in Sarawak, Sabah, and Brunei". *PLoS ONE* 8(7): e69679. https://doi.org/10.1371/journal.pone.0069679

Evans, Luke J., Gregory P. Asner, and Benoit Goossens. 2018. "Protected Area Management Priorities Crucial for the Future of Bornean Elephants." *Biological Conservation* 221 (May): 365–73. https://doi.org/10.1016/j.biocon.2018.03.015.

Fernandes, Pedro José Farias, Luiz Felipe de Almeida Furtado, and Raphael e Silva Girão. 2014. "Change vector analysis to detect deforestation and land use/land cover change in Brazilian Amazon." *Brazilian Geographical Journal: Geosciences and Humanities research medium* 5 (2): 371–87. https://dialnet.unirioja.es/servlet/articulo?codigo=4995484.

Gaveau, David L. A., Douglas Sheil, Husnayaen, Mohammad A. Salim, Sanjiwana Arjasakusuma, Marc Ancrenaz, Pablo Pacheco, and Erik Meijaard. 2016. “Rapid Conversions and Avoided Deforestation: Examining Four Decades of Industrial Plantation Expansion in Borneo.” *Scientific Reports* 6 (September): 32017. https://doi.org/10.1038/srep32017.

Gorelick, Noel, Matt Hancher, Mike Dixon, Simon Ilyushchenko, David Thau, and Rebecca Moore. 2017. “Google Earth Engine: Planetary-Scale Geospatial Analysis for Everyone.” *Remote Sensing of Environment, Big Remotely Sensed Data: tools, applications and experiences*, 202 (December): 18–27. https://doi.org/10.1016/j.rse.2017.06.031.

Hansen, Matthew C., Stephen V. Stehman, Peter V. Potapov, Thomas R. Loveland, John R. G. Townshend, Ruth S. DeFries, Kyle W. Pittman, et al. 2008. “Humid Tropical Forest Clearing from 2000 to 2005 Quantified by Using Multitemporal and Multiresolution Remotely Sensed Data.” *Proceedings of the National Academy of Sciences* 105 (27): 9439–44. https://doi.org/10.1073/pnas.0804042105.

Hansen, Matthew C., and Thomas R. Loveland. 2012. “A Review of Large Area Monitoring of Land Cover Change Using Landsat Data.” *Remote Sensing of Environment, Landsat Legacy Special Issue*, 122 (July): 66–74. https://doi.org/10.1016/j.rse.2011.08.024.

Hansen, Matthew C., Alexander Krylov, Alexandra Tyukavina, Peter V. Potapov, Svetlana Turubanova, Bryan Zutta, Suspense Ifo, Belinda Margono, Fred Stolle, and Rebecca Moore. 2016. “Humid Tropical Forest Disturbance Alerts Using Landsat Data.” *Environmental Research Letters* 11 (3): 034008. https://doi.org/10.1088/1748-

9326/11/3/034008.

Hammer, Dan, Robin Kraft, and David Wheeler. 2014. “Alerts of Forest Disturbance from MODIS Imagery.” *International Journal of Applied Earth Observation and Geoinformation* 33 (December): 1–9. https://doi.org/10.1016/j.jag.2014.04.011.

Houghton, R. A., Brett Byers, and Alexander A. Nassikas. 2015. “A Role for Tropical Forests in Stabilizing Atmospheric CO2.” *Nature Climate Change* 5 (12): 1022–23. https://doi.org/10.1038/nclimate2869.

Houborg, Rasmus, and Matthew F. McCabe. 2018. “A Cubesat Enabled Spatio-Temporal Enhancement Method (CESTEM) Utilizing Planet, Landsat and MODIS Data.” *Remote Sensing of Environment* 209 (May): 211–26. https://doi.org/10.1016/j.rse.2018.02.067.

Jacquemard, J.C. 2013. *Le palmier à huile en plantation villageoise*, Versailles : Quae ;

Joshi, Neha, Matthias Baumann, Andrea Ehammer, Rasmus Fensholt, Kenneth Grogan, Patrick Hostert, Martin Rudbeck Jepsen, et al. 2016. “A Review of the Application of Optical and Radar Remote Sensing Data Fusion to Land Use Mapping and Monitoring.” *Remote Sensing* 8 (1): 70. https://doi.org/10.3390/rs8010070.

Khun, Vathana, and Nophea Sasaki. 2014. “Re-Assessment of Forest Carbon Balance in Southeast Asia: Policy Implications for REDD+.” *Low Carbon Economy* 05 (04): 153. https://doi.org/10.4236/lce.2014.54016.

Knipling, Edward B. 1970. “Physical and Physiological Basis for the Reflectance of Visible and Near-Infrared Radiation from Vegetation.” *Remote Sensing of Environment* 1 (3): 155–59. https://doi.org/10.1016/S0034-4257(70)80021-9.

Koh, Lian Pin, Jukka Miettinen, Soo Chin Liew, and Jaboury Ghazoul. 2011. "Remotely Sensed Evidence of Tropical Peatland Conversion to Oil Palm." *Proceedings of the National Academy of Sciences* 108 (12): 5127–32. https://doi.org/10.1073/pnas.1018776108.

Lê T.T. 2015. "Extraction d'Informations de changement à partir des Séries Temporelles d'Images Radar à Synthèse d'Ouverture." PhD diss., Université de Grenoble Alpes, STIC Traitement de l'Information, 174 p.

Lehmann, Eric A., Peter Caccetta, Kim Lowell, Anthea Mitchell, Zheng-Shu Zhou, Alex Held, Tony Milne, and Ian Tapley. 2015. "SAR and Optical Remote Sensing: Assessment of Complementarity and Interoperability in the Context of a Large-Scale Operational Forest Monitoring System." Remote Sensing of Environment 156 (January): 335–48. https://doi.org/10.1016/j.rse.2014.09.034.

Lopes A., Nezry E., Touzi R., Laur H..1990. "Maximum a posteriori speckle filtering and first order texture models in SAR images" Paper presented at Geoscience and Remote Sensing Symposium, 1990. IGARSS '90. 'Remote Sensing Science for the Nineties'., 10th Annual International 2409-2412 https://doi.org/10.1109/IGARSS.1990.689026

Maghsoudi, Yasser, Michael J. Collins, and Donald Leckie. 2012. "Speckle Reduction for the Forest Mapping Analysis of Multi-Temporal Radarsat-1 Images." International Journal of Remote Sensing 33 (5): 1349–59. https://doi.org/10.1080/01431161.2011.568530.

Malila, William. 1980. "Change Vector Analysis: An Approach for Detecting Forest Changes with Landsat." LARS Symposia, January.

https://docs.lib.purdue.edu/lars_symp/385.

Mandanici, Emanuele, and Gabriele Bitelli. 2016. “Preliminary comparison of Sentinel-2 and Landsat 8 Imagery for a Combined Use.” *Remote Sensing* 8 (12): 1014. https://doi.org/10.3390/rs8121014.

May-Tobin, C., Boucher, D., Decker, E., Hurowitz, G., Martin, J., Mulik, K., Roquemore, S., Stark, A. 2002. *Recipes for Sucess. Solutions for Deforestation-Free Vegetable Oils*. Union of Concerned Scientists (UCS), MA, U.S.A. https://www.ucsusa.org/sites/default/files/legacy/assets/documents/global_warming/Recipes-for-Success.pdf

Miettinen, Jukka, Chenghua Shi, and Soo Chin Liew. 2016. “Land Cover Distribution in the Peatlands of Peninsular Malaysia, Sumatra and Borneo in 2015 with Changes since 1990.” Global Ecology and Conservation 6 (April): 67–78. https://doi.org/10.1016/j.gecco.2016.02.004.

MODIS Collection 6 NRT Hotspot / Active Fire Detections MCD14DL. Available on-line https://earthdata.nasa.gov/firms. DOI: 10.5067/FIRMS/MODIS/MCD14DL.NRT.006

Olofsson, Pontus, Giles M. Foody, Martin Herold, Stephen V. Stehman, Curtis E. Woodcock, and Michael A. Wulder. 2014. “Good Practices for Estimating Area and Assessing Accuracy of Land Change.” Remote Sensing of Environment 148 (May): 42–57. https://doi.org/10.1016/j.rse.2014.02.015.

Phua, Mui-How, Satoshi Tsuyuki, Naoyuki Furuya, and Jung Soo Lee. 2008. “Detecting Deforestation with a Spectral Change Detection Approach Using Multitemporal Landsat Data: A Case Study of Kinabalu Park, Sabah, Malaysia.”

Journal of Environmental Management 88 (4): 784–95. https://doi.org/10.1016/j.jenvman.2007.04.011.

Planet 2018. Planet Application Program Interface: In Space for Life on Earth. San Francisco, CA. https://api.planet.com.

Qi, Zhixin, Anthony Gar-On Yeh, Xia Li, and Xiaohu Zhang. 2015. "A Three-Component Method for Timely Detection of Land Cover Changes Using Polarimetric SAR Images." ISPRS Journal of Photogrammetry and Remote Sensing, Multitemporal remote sensing data analysis, 107 (September): 3–21. https://doi.org/10.1016/j.isprsjprs.2015.02.004.

Quegan S., Le Toan T., Yu J. J., Jiong, Ribbes F., Floury N. 2000. "Multitemporal ERS SAR analysis applied to forest mapping." *IEEE Transactions on Geoscience and Remote Sensing* 38 (2): 741–753.

Reiche, Johannes, Eliakim Hamunyela, Jan Verbesselt, Dirk Hoekman, and Martin Herold. 2018. "Improving Near-Real Time Deforestation Monitoring in Tropical Dry Forests by Combining Dense Sentinel-1 Time Series with Landsat and ALOS-2 PALSAR-2." *Remote Sensing of Environment* 204 (January): 147–61. https://doi.org/10.1016/j.rse.2017.10.034.

Reymondin, Louis, Andrew Jarvis, Andres Perez-Uribe, Jerry Touval, Karolina Argote, Julien Rebetez, Edward Guevara, and Mark Mulligan. 2012. "Terra-i: A methodology for near real-time monitoring of habitat change at continental scales using MODIS-NDVI and TRMM" n.d. *ResearchGate*. Accessed July 9, 2018. https://doi.org/10.13140/RG.2.2.15618.99520

Rival, A., Levang, P. 2013. *La palme des controverses: palmier à huile et enjeux du*

développement, Versailles: Éditions Quae, 98 p. (Essais),

Rouse, J. W. 1974. “Monitoring the Vernal Advancement and Retrogradation (Green Wave Effect) of Natural Vegetation.” https://ntrs.nasa.gov/search.jsp?R=19740022555.Song, Conghe, Curtis E. Woodcock, Karen C. Seto, Mary Pax Lenney, and Scott A. Macomber. 2001. “Classification and Change Detection Using Landsat TM Data: When and How to Correct Atmospheric Effects?” Remote Sensing of Environment 75 (2): 230–44. https://doi.org/10.1016/S0034-4257(00)00169-3.

Skerman, P. J. 1982. Les legumineuses fourrageres tropicales. Food & Agriculture Org.

Storey, James, David P. Roy, Jeffrey Masek, Ferran Gascon, John Dwyer, and Michael Choate. 2016. “A Note on the Temporary Misregistration of Landsat-8 Operational Land Imager (OLI) and Sentinel-2 Multi Spectral Instrument (MSI) Imagery.” Remote Sensing of Environment 186 (December): 121–22. https://doi.org/10.1016/j.rse.2016.08.025.

Surre, C. Ziller, R. 1963. Le palmier à huile. Paris: G. P. Maisonneuve & Larose.

Thonfeld, Frank, Hannes Feilhauer, Matthias Braun, and Gunter Menz. 2016. “Robust Change Vector Analysis (RCVA) for Multi-Sensor Very High Resolution Optical Satellite Data.” *International Journal of Applied Earth Observation and Geoinformation* 50 (August): 131–40. https://doi.org/10.1016/j.jag.2016.03.009.

Verheye, W. 2010. *Growth and Production of Oil Palm*. Verheye, W. (ed.), Land Use, Land Cover and Soil Sciences. Encyclopedia of Life Support Systems (EOLSS), UNESCO-EOLSS Publishers, Oxford, UK. http://www.eolss.net

Vermote, E., R. Wolfe. MOD09GA MODIS/Terra Surface Reflectance Daily L2G Global 1kmand 500m SIN Grid V006. 2015, distributed by NASA EOSDIS LP DAAC, https://doi.org/10.5067/MODIS/MOD09GA.006

Wakker, E., S. Watch, and J. de Rozario. 2004. "Greasy Palms: The Social and Ecological Impacts of Large-Scale Oil Palm Plantation Development in Southeast Asia." Greasy Palms: The Social and Ecological Impacts of Large-Scale Oil Palm Plantation Development in Southeast Asia. https://www.cabdirect.org/cabdirect/abstract/20056701996.Wheeler, David, Brook Guzder-Williams, Rachael Petersen, and David Thau. 2018. "Rapid MODIS-Based Detection of Tree Cover Loss." *International Journal of Applied Earth Observation and Geoinformation* 69 (July): 78–87. https://doi.org/10.1016/j.jag.2018.02.007.

FIGURES

Figure 1: (a) Study area locations, (b) Daily percentage cloud cover and the polynomial trend line for Sabah, which was calculated from ten years of MODIS surface reflectance products 'state_1km', MODIS, MOD09GA, 2017 (Vermote et al. 2015).

Figure 2: Availability of images over Malaysia and Indonesia for Landsat-8, Sentinel-1 and Sentinel-2.

Figure 3: Analysis method flowchart. The method performs the simultaneous analyses of 3 sensors to detect deforestation.

Figure 4: (a) Representation of change vector in 2-band radiometric change space (for Sentinel-1), (b) Representation of change vector in 3-band radiometric change space (for Sentinel-2 and Landsat-8).

Figure 5: Figure (a) illustrates the VV (vertical/vertical) and VH (vertical/horizontal) bands for Sentinel-1. Figure (b) corresponds to Sentinel-2 sensors, with (b)(i) angle Band 4/ Band 8A, (b)(ii) angle Band 4/ Band 11 and (b)(iii) angle Band 8A/ Band 11. Figure (c) corresponds to Landsat-8 sensors, with (c)(i) angle Band 4/Band 5, (c)(ii) angle Band 4/ Band 6 and (c)(iii) angle Band 5/ Band 6. Polar coordinate plots that were obtained by applying CVA, against 15 reference forest polygon averages. Green represent no change, red represent deforestation events, and blue are samples covered by cloud. The blue polygon indicates the deforestation threshold. Black dash polygons represent other example of thresholds.

Figure 6: Spatial accuracy (omission and commission errors) of the deforestation class as a function of four examples of threshold values, separately for (a) Landsat-8, (b) Sentinel-2 and (c) Sentinel-1. Thresholds annotation correspond to the parameters shown in figure 5. Surrounded thresholds were used in our study.

Figure 7: (a) Deforestation events detected at the multi-sensor level during the 17 months monitoring period in Sabah. (b) Deforestation events detected at the multi-sensor level during the 5 months monitoring period in Sumatra study area.

Figure 8: Comparative analysis of deforestation omission, and commission error for the three sensors corresponding to the best thresholds. (a) Corresponds to the polygons level

approach, and (b) to the pixel-based adjusted area. (c) Represent the multi-sensor analysis in pixel-based adjusted area and its comparison with GLAD alert detection (Hansen et al. 2016). Numerical values on the histogram bars represent exact percentage values.

Figure 9: Days of the first detection after deforestation events (estimates) across sensors, for (a) high cloud-cover season and (b) low cloud-cover season. The thick horizontal line within the box-plots represents the median (50^{th} percentile) of each sensor. The box-plots themselves delimit the first and third quartiles (25^{th} and 75^{th} percentiles) and the whiskers (vertical dashed lines) indicate the 10^{th} and 90^{th} percentiles. Open circles represent outliers (i.e. values that are beyond 1.5 times the interquartile range.

Figure 10: Density of deforestation events that were detected as a function of time following deforestation (estimated). These results allowed us to visualise the distribution of detection responses before and after deforestation. Zero is the estimated first date of forest cover loss.

Figure 11: Number of validation polygons (as percentages) as a function of the number of times that they were detected over a period of 100 days following forest clearing.

Figure 12: (a, b, c) Examples of drone photographs that were taken 9 May 2018. (d) Illustration of deforestation detection: In red, pixels detected as deforested by our method, between 1 January and 31 May 2018, over a Planet image of 18 February 2018. Points are the position of the drone pictures, green points are forest (a), and pink points are bare soil (b and c).

Figure 13: Comparative analysis of deforestation omission and commission errors and overall accuracy of the method presented in this paper versus that provided by GLAD forest alert detection (Hansen et al. 2016). Numerical values on the histogram bars represent exact percentage values.